Kirchhoff's Laws as a Finite Volume Method for the Planar Maxwell Equations

Harish S. Bhat and Braxton Osting

Abstract—Beginning with Maxwell's equations for the (H_1, H_2, E) polarized mode in an inhomogeneous planar medium, we derive a finite volume method that we recognize as Kirchhoff's laws for a corresponding circuit consisting of inductors, capacitors, and resistors. This association automatically gives local charge and energy conservation. The method is implemented and used to find the steady-state solution for two test problems. By comparison with the exact solution for the homogeneous medium problem, the method is shown to be linearly convergent.

Index Terms—Finite volume methods, Maxwell equations, Helmholtz equation, Circuit modeling, Equivalent circuits

I. INTRODUCTION

MAXWELL'S equations for the (H_1, H_2, E) polarized mode in a planar, inhomogeneous medium with permittivity $\epsilon(x, y)$ and permeability $\mu(x, y)$ are

$$\mu \partial_t \Lambda = -\nabla E, \qquad \Lambda = (-H_2, H_1) \tag{1a}$$

$$\epsilon \partial_t E = -\operatorname{div} \Lambda. \tag{1b}$$

Let $\Omega = [0, M] \times [0, L]$ be the rectangular region occupied by the medium. Let $\overline{\Gamma} = \{0\} \times [0, L]$ be the left boundary of Ω. Suppose that on $\overline{\Gamma}$, we have harmonic forcing at frequency α:

$$E(0, y, t) = f(0, y)e^{2\pi \iota \alpha t}. \tag{1c}$$

On the remaining three sides of the boundary, we impose impedance or Leontovich boundary conditions:

$$\Lambda(x, y, t) \cdot \hat{\mathbf{n}} = \sigma(x, y)E(x, y, t), \quad (x, y) \in \partial\Omega \setminus \overline{\Gamma}, \tag{1d}$$

where $\partial\Omega$, $\hat{\mathbf{n}}$, and $\sigma(x, y)$ denote the boundary of Ω, the unit outward normal, and the conductance on the boundary.

In this paper, we accomplish the following goals:

1) We show that a finite volume discretization of (1) results in Kirchhoff's laws of voltage and current for a particular circuit consisting of inductors, capacitors, and resistors.
2) By comparing finite volume solutions of (1) for constant ϵ and μ with exact solutions obtained via separation of variables, we numerically establish first-order convergence.

H. S. Bhat is with the School of Natural Sciences, University of California, Merced, Merced, CA 95343 USA email: hbhat@ucmerced.edu

B. Osting is with the Department of Applied Physics and Applied Mathematics, Columbia University, New York, NY 10027 USA email: bro2103@columbia.edu

A. Relationship to previous work

The idea of demonstrating equivalent circuits whose continuum limit yields Maxwell's equations is quite old [1]–[4]. These early works predate the widespread use of digital computers to solve differential/integral equations.

Since then, when a new numerical method for Maxwell's equations has been introduced, the corresponding equivalent circuit has been explored, often as a way to gain physical insight useful for modeling purposes [5, Chap. 1]. One of the first papers proposing an equivalent circuit for the FDTD discretization was [6]. Equivalent circuits for the Finite Element Method and the Method of Moments have been described in [7] and [8, Chap. 5], respectively. For the Transmission Line Matrix method [5], [9], [10] and the Spatial Network Method [11], [12], equivalent circuits feature prominently.

The finite volume (FV) method appeared in computational electromagnetics in the late 1980s [13]–[16]. More recent work indicates that FV methods may hold an advantage over other methods for problems with large variations in the material parameters and sub-grid scale variations in the fields [17]–[20]. Note that the convergence of at least two versions of the FV method has been proven rigorously [21]–[24].

Despite the fact that the FV method has been employed successfully for over 20 years, and unlike the situation for any of the other popular methods for solving Maxwell's equations, there has to date been no discussion in the literature of an equivalent circuit for the FV discretization. We find two main benefits of carefully deriving an equivalent circuit formulation of the FV discretization. First, we obtain precise formulas that relate the local inductance, capacitance, and boundary conductance of the circuit to *spatial averages* of their continuum counterparts: $\mu(x, y)$, $\epsilon(x, y)$ and $\sigma(x, y)$, respectively. Second, relating the FV discretization to Kirchhoff's laws for a circuit automatically yields local energy and charge conservation, in addition to global energy and charge functionals that are natural discretizations of the continuum energy and charge functionals for Maxwell's equations.

From the point of view of using FV to analyze a two-dimensional case of Maxwell's equations, our work is most similar to [25]. We solve (1) in steady-state for an arbitrary frequency $2\pi\alpha$ in (1c); this amounts to finding the frequency-domain solution, which is exactly the goal of the frequency-domain FV method proposed in [20]. In the present work, we are not concerned with issues related to unstructured, adaptive, or hybridized meshes [26]–[28], though we note here that our derivation can be generalized in this direction.
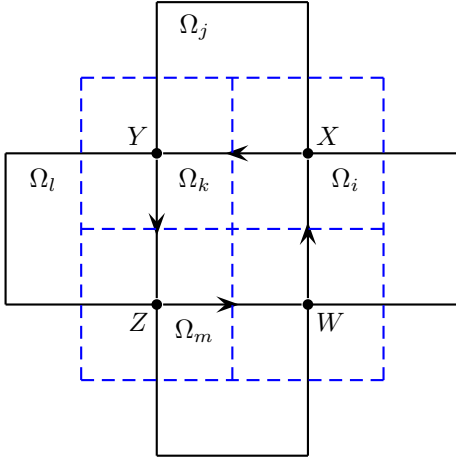
Fig. 1. Cell diagram of finite volume discretization for an interior cell Ω_k. The blue dashed lines indicate the dual graph.

II. FINITE VOLUME DISCRETIZATION OF PLANAR MAXWELL'S EQUATIONS

In this section, we derive a finite volume method discretization for (1). We tile our rectangular domain Ω with small square cells, m in the vertical direction and n in the horizontal direction. We define the *charge* Q_k in the cell Ω_k:

$$Q_k(t) := \int_{\Omega_k} \epsilon(x,y)E(x,y,t)\,\mathrm{d}\mathbf{x}. \tag{2}$$

We define the *capacitance* C_k to be the scaled permittivity in the cell Ω_k:

$$C_k := \frac{1}{\eta}\int_{\Omega_k}\epsilon(x,y)\,\mathrm{d}\mathbf{x}, \tag{3}$$

where $\eta > 0$ is a characteristic length scale in the out-of-plane direction. Next, we define the *voltage* $V_k(t) = Q_k(t)/C_k$, so

$$C_k\dot{V}_k = \int_{\Omega_k}\partial_t(\epsilon E)\,\mathrm{d}\mathbf{x} = -\int_{\Omega_k}\mathrm{div}\,\Lambda\,\mathrm{d}\mathbf{x} = -\oint_{\partial\Omega_k}\Lambda\cdot\mathbf{n}\,\mathrm{d}\ell. \tag{4}$$

Let us assume for a moment that Ω_k is an interior cell, so that $\partial\Omega_k$ has no intersection with $\partial\Omega$. As shown in Figure 1, Ω_k has four neighboring cells labeled Ω_i, Ω_j, Ω_l, and Ω_m, the right, up, left, and down neighbors, respectively. We label the four corners of Ω_k as W, X, Y, and Z. With this notation,

$$C_k\dot{V}_k = \int_{\overrightarrow{WX}}H_2\,\mathrm{d}\ell + \int_{\overrightarrow{XY}}(-H_1)\,\mathrm{d}\ell$$
$$+ \int_{\overrightarrow{YZ}}(-H_2)\,\mathrm{d}\ell + \int_{\overrightarrow{ZW}}H_1\,\mathrm{d}\ell. \tag{5}$$

Now let us define the currents. In general, when we have two neighboring cells Ω_k and Ω_i that are separated by a vertical segment γ, if Ω_k is to the left of Ω_i, then we define the *horizontal current*

$$I_{k,i} := \int_\gamma(-H_2)\,\mathrm{d}\ell. \tag{6}$$

In general, when we have two neighboring cells Ω_k and Ω_j that are separated by a horizontal segment γ, if Ω_k is below

Ω_j, then we define the *vertical current*

$$I_{k,j} := \int_\gamma H_1\,\mathrm{d}\ell. \tag{7}$$

Note that the right-hand sides of (5), (6), and (7) all involve line integrals of scalar fields, which are all independent of parametrization.

With these conventions, we have

$$C_k\dot{V}_k = -I_{k,i} - I_{k,j} + I_{l,k} + I_{m,k}. \tag{8}$$

Note that this equation says that at each lattice node, the sum of incoming currents must equal the sum of outgoing currents, implying local charge conservation.

We define the *inductance* of the segment γ as

$$L_\gamma := \frac{\eta}{|\gamma|}\int_\gamma\mu\,\mathrm{d}\ell. \tag{9}$$

Let us check how the currents evolve in time. We compute

$$\dot{I}_{k,i} = -\int_\gamma\frac{\partial_x E}{\mu}\,\mathrm{d}\ell \approx -\frac{\eta}{L_\gamma}\int_\gamma\partial_x E\,\mathrm{d}\ell \tag{10a}$$

$$\approx -\frac{\eta}{L_\gamma}\left(|\Omega_i|^{-1}\int_{\Omega_i}E\,\mathrm{d}\mathbf{x} - |\Omega_k|^{-1}\int_{\Omega_k}E\,\mathrm{d}\mathbf{x}\right) \tag{10b}$$

$$\approx \frac{1}{L_\gamma}(V_k - V_i). \tag{10c}$$

Let us explain the sequence of approximations made above:

- In (10a), we replace μ by its segment average L_γ/η.
- To approximate the flux between cells in (10a), the integral $\int_\gamma\partial_x E\,\mathrm{d}\ell$ is approximated by the value of $\partial_x E$ evaluated at the midpoint of γ, a second-order accurate finite-difference formula is applied using the values of E at the center of the cells Ω_q and Ω_p, and then these values are replaced by the cell averages. This is the main finite volume approximation [29].
- To go from (10b) to (10c), we replace ϵ by its cell average, which gives us

$$V_k = \frac{Q_k}{C_k} = \frac{\int_{\Omega_k}\epsilon E\,\mathrm{d}\mathbf{x}}{\eta^{-1}\int_{\Omega_k}\epsilon\,\mathrm{d}\mathbf{x}} \approx \frac{\eta}{|\Omega_k|}\int_{\Omega_k}E\,\mathrm{d}\mathbf{x}. \tag{11}$$

Using analogous approximations, we compute

$$\dot{I}_{k,j} \approx \frac{1}{L_\gamma}(V_k - V_j). \tag{12}$$

For an interior cell Ω_k, (8), (10), and (12) are Kirchhoff's laws of voltage and current for a regular square lattice of inductors and capacitors [30], [31].

A. Boundary conditions

To handle boundary condition (1c) on $\overline{\Gamma}$, we use a column of ghost cells. Each ghost cell, where the electric field is prescribed, is directly to the left of a cell in the first column, where the electric field is an unknown. Let $\gamma \subset \overline{\Gamma}$ be the right boundary of the ghost cell. We compute the voltage of the ghost cell using (11):

$$V_k \approx \frac{\eta}{|\Omega_k|}\int_{\Omega_k}E\,\mathrm{d}\mathbf{x} \approx \frac{\eta}{|\gamma|}\int_\gamma E\,\mathrm{d}\ell = \tilde{V}_k e^{2\pi\iota\alpha t}, \tag{13}$$

with

$$\tilde{V}_k = \eta \left(\frac{1}{|\gamma|} \int_\gamma f(y)\,dy \right).$$

The ghost cells yield n new horizontal currents $I_{p,q}$, each of which satisfies an equation of the form (10). Each such equation involves one unknown and one prescribed voltage.

If the top, right, or bottom boundary of Ω_k intersects $\partial\Omega$, then we apply the other boundary condition (1d). Let $\gamma = \partial\Omega_k \cap \partial\Omega$. Then going back to (4), we find

$$C_k \dot{V}_k = -\int_\gamma \Lambda \cdot \mathbf{n}\,\mathrm{d}\ell - \int_{\partial\Omega_k \setminus \gamma} \Lambda \cdot \mathbf{n}\,\mathrm{d}\ell \qquad (14)$$

$$= -\int_\gamma \sigma E\,\mathrm{d}\ell - \int_{\partial\Omega_k \setminus \gamma} \Lambda \cdot \mathbf{n}\,\mathrm{d}\ell$$

The second line integral in (14) can be evaluated in the same way as (5) above; we focus on the first line integral. We write

$$\int_\gamma \sigma E\,\mathrm{d}\ell \approx \left(\frac{1}{|\gamma|} \int_\gamma E\,\mathrm{d}\ell \right) \left(\int_\gamma \sigma\,\mathrm{d}\ell \right)$$

$$\approx \left(\frac{\eta}{|\Omega_k|} \int_{\Omega_k} E\,\mathrm{d}\mathbf{x} \right) \left(\frac{1}{\eta} \int_\gamma \sigma\,\mathrm{d}\ell \right) \approx V_k G_k,$$

where G_k is the *conductance*

$$G_k := \frac{1}{\eta} \int_\gamma \sigma\,\mathrm{d}\ell. \qquad (15)$$

Note that if $\sigma = 0$, then (1d) and (1a) imply $\nabla E \cdot \hat{\mathbf{n}} = 0$, a perfectly insulating boundary condition. On the other hand, if $\sigma = \infty$, then (1d) implies $E = 0$, a perfectly conducting boundary condition. In this paper, we choose σ to approximate outgoing boundary conditions, which are obtained as follows.

Dotting (1a) with $\hat{\mathbf{n}}$ and then using (1d), we find that on $\partial\Omega \setminus \overline{\Gamma}$,

$$\partial_t E + \frac{1}{\mu\sigma} \nabla E \cdot \mathbf{n} = 0.$$

At each $(x, y) \in \partial\Omega \setminus \overline{\Gamma}$, the value of $\sigma(x, y)$ for which this equation is the Engquist-Majda outgoing condition [32] is

$$\sigma(x, y) = \sqrt{\epsilon(x, y)/\mu(x, y)}. \qquad (16)$$

B. Remark

In Appendix A, we show that the (H_1, H_2, E) polarized mode described by (1) is an exact solution of the fully three-dimensional Maxwell's equations for a physical system described by two horizontally infinite parallel plates that are separated vertically by the distance $\eta > 0$. All the definitions made above (e.g., charge, capacitance, resistance, etc.) can be derived in a physically consistent fashion using the setup in Appendix A. One may also make these definitions on the grounds that the quantities being derived have the correct units.

C. Assembling the discretized system

Discretization gives us a two-dimensional rectangular lattice with m rows and n columns, which we represent as an oriented graph, c.f. [33, Chap. 13]. This graph is the dual graph of the finite volume mesh as shown in Fig. 1. Nodes represent capacitors and edges represent inductors. The direction or orientation of the edge represents the direction of positive current flow through the associated inductor.

In a lattice of size $m \times n$, there are mn nodes and $(2m - 1)n$ edges, mn horizontal ones and $(m - 1)n$ vertical ones. We let $\mathfrak{N} = \{1, 2, \ldots, mn\}$ denote the set of all nodes, and $\mathfrak{E} = \{1, 2, \ldots, (2m - 1)n\}$ denote the set of all edges. Let $\mathbf{C}$ be a vector of size mn such that C_j is the capacitance at node j. Let $\mathbf{L}$ be a vector of size $(2m - 1)n$ such that L_j is the inductance at edge j. We partition $\mathbf{L}$ into horizontal and vertical inductances by writing $\mathbf{L} = [\mathbf{L}_h, \mathbf{L}_v]$. At time t, $V_j(t)$ and $I_k(t)$ are, respectively, the voltage across capacitor j and the current through inductor k. By $\mathbf{V}(t)$ and $\mathbf{I}(t)$ we denote the vectors of all voltages and currents, respectively.

Of the horizontal edges, there are m boundary edges that form a subset $\Gamma \subset \mathfrak{E}$, each of which is incident upon only one node and corresponds to a ghost cell to the left of the domain Ω. Specifically, Γ is the left-most column of horizontal edges. All other edges in the graph are incident upon two nodes. In general, we think of an edge as an ordered pair (i_1, i_2), where $i_k \in \mathfrak{N}$. The direction of the edge is given by the ordering of these numbers, so that i_1 is the tail and i_2 is the head of (i_1, i_2). For a boundary edge j that is incident only upon node i, we write $j = (\emptyset, i)$.

We let $\mathfrak{B}$ denote the $|\mathfrak{N}| \times |\mathfrak{E}| = mn \times (2m-1)n$ incidence matrix of the oriented graph for our circuit. We have

$$\mathfrak{B}_{ij} = \begin{cases} 1 & \text{if } j = (i', i) \text{ for some } i' \in \mathfrak{N} \cup \{\emptyset\} \\ -1 & \text{if } j = (i, i') \text{ for some } i' \in \mathfrak{N} \\ 0 & \text{otherwise.} \end{cases}$$

In addition to the structure described already, the lattice also has resistors and forcing along the boundary. We represent the set of nodes connected to resistors by $\mathfrak{G} \subset \mathfrak{N}$, and let G_i be the conductance of node $i \in \mathfrak{G}$. We then extend G_i by defining $G_i \equiv 0$ for all $i \in \mathfrak{N} \setminus \mathfrak{G}$, so that $\mathbf{G} = (G_1, \ldots, G_{mn})$ is a vector of size $|\mathfrak{N}| = mn$.

Let $N = |\mathfrak{N}| + |\mathfrak{E}| = (3m - 1)n$. Then we define the $|\Gamma| \times N = m \times (3m-1)n$ projection matrix P_Γ by $(P_\Gamma)_{ij} = 1$ if $\Gamma_i = j$ and $(P_\Gamma)_{ij} = 0$ otherwise. Note that because $\Gamma_i \in \mathfrak{E}$, the final mn columns of P_Γ are all zero. The forcing applied at edges Γ is

$$\mathbf{W}(t) = P_\Gamma^t \mathbf{f} e^{2\pi\iota\alpha t}.$$

The frequency α is the same α in the boundary condition (1c). The vector $\mathbf{f} = (f_1, \ldots, f_m) \in \mathbb{C}^{|\Gamma|}$ is arranged as follows: each edge $i \in \Gamma$ is of the form $(\emptyset, k')$ for some $k' \in \mathfrak{N}$. We set f_i equal to $\tilde{V}_k$ as defined in (13), where Ω_k is the ghost cell to the left of cell $\Omega_{k'}$.

The finite volume scheme from the previous section, which we have already noted is equivalent to Kirchhoff's Laws on an inductor-capacitor lattice, can now be written in the following matrix-vector form:

$$\mathrm{diag}(\mathbf{L}) \frac{\mathrm{d}\mathbf{I}}{\mathrm{d}t} = -\mathfrak{B}^t \mathbf{V} + \mathbf{W} \qquad (17a)$$

$$\mathrm{diag}(\mathbf{C}) \frac{\mathrm{d}\mathbf{V}}{\mathrm{d}t} = \mathfrak{B}\mathbf{I} - \mathrm{diag}(\mathbf{G})\mathbf{V}. \qquad (17b)$$

D. Steady-state solution of the discretized equation

Define $\mathbf{z}(t) = (\mathbf{I}(t), \mathbf{V}(t))$ so for each t, $\mathbf{z}(t) \in \mathbb{C}^N$. Define

$$M = \begin{bmatrix} 0 & -\mathfrak{B}^t \\ \mathfrak{B} & -\mathrm{diag}(\mathbf{G}) \end{bmatrix},$$

Then the system (17) can be written in the form

$$\mathrm{diag}(\mathbf{L}, \mathbf{C})\dot{\mathbf{z}}(t) = M\mathbf{z}(t) + P_\Gamma^t \mathbf{f} e^{2\pi\iota\alpha t}. \tag{18}$$

Consider the steady-state solution $\mathbf{z}(t) = \mathbf{u}e^{2\pi\iota\alpha t}$. Inserting this into (18), we derive

$$\mathbf{u} = (2\pi\iota\alpha\,\mathrm{diag}(\mathbf{L}, \mathbf{C}) - M)^{-1} P_\Gamma^t \mathbf{f}. \tag{19}$$

E. Discussion

1) The matrix $(2\pi\iota\alpha\,\mathrm{diag}(\mathbf{L}, \mathbf{C}) - M)$ will be invertible if and only if $2\pi\iota\alpha$ is not an eigenvalue of $\mathrm{diag}(\mathbf{L}, \mathbf{C})^{-1}M$. Note that if all nodes are resistive, i.e., if $G_k > 0$ for for all $i \in \mathfrak{N}$, then the spectrum of $\mathrm{diag}(\mathbf{L}, \mathbf{C})^{-1}M$ has strictly negative real part, implying that (19) can be computed for all real α.

2) Using Matlab on a desktop computer with 4GB of RAM, (19) can easily be solved for $m, n \le 400$.

3) We have formulated the circuit as an oriented graph in order to write the equations compactly and take advantage of the graph-theoretic interpretation of the incidence matrix $\mathfrak{B}$, which appears naturally in Kirchhoff's laws. Though we have formulated the problem for an $m \times n$ rectangular lattice, the graph-theoretic framework easily accommodates other topologies.

4) Inserting (16) into (15), we find that at a boundary node $i \subset \mathfrak{G}$, we have the impedance-matched value of the conductance,

$$G_i = \frac{|\gamma|}{|\Omega_i|^{1/2}} \sqrt{\frac{C_i}{L_j}}, \tag{20}$$

where $j \in \mathfrak{E}$ is the edge incident on node i that is normal to the boundary, and γ is the segment that is dual to edge j. In the case where all cells are identical squares, we have $|\gamma| = |\Omega_i|^{1/2}$.

III. CONSERVATION PROPERTIES OF THE CONTINUOUS AND DISCRETE SYSTEMS

It is instructive to calculate the time evolution of the total energy for the Maxwell system (1):

$$\frac{d}{dt}\frac{1}{2}\int_\Omega \epsilon|E|^2 + \mu\|\Lambda\|^2\,\mathrm{d}A = -\Re\int_{\partial\Omega} E^*\Lambda \cdot \mathbf{n}\,\mathrm{d}\ell$$
$$= -\Re\int_{\overline{\Gamma}} f(y)e^{-2\pi\iota\alpha t}H_2\,\mathrm{d}\ell - \int_{\partial\Omega\backslash\overline{\Gamma}} \sigma|E|^2\,\mathrm{d}\ell. \tag{21}$$

This says that the rate of change of energy equals the power forced in through the left boundary minus the power dissipated through the other three sides of the medium. It is clear that power is dissipated at a rate proportional to σ.

We also compute the time-evolution of the total charge of the system

$$\frac{\mathrm{d}}{\mathrm{d}t}\int_\Omega \epsilon E\,\mathrm{d}x = -\int_{\overline{\Gamma}} \Lambda \cdot \mathbf{n}\,\mathrm{d}x - \int_{\partial\Omega\backslash\overline{\Gamma}} \sigma E\,\mathrm{d}x. \tag{22}$$

The interpretation of this equation is that the rate of change of charge equals the current entering the domain on the left boundary minus the current exiting the domain on the other three sides. Again, the outgoing current is proportional to σ.

The association of the finite volume discretized system as Kirchhoff's laws for a circuit allows for natural definitions of discrete energy and charge. The rate of change of the total energy of the discrete system can be calculated using (17):

$$\frac{1}{2}\frac{\mathrm{d}}{\mathrm{d}t}\left(\mathbf{V}^*\mathrm{diag}(\mathbf{C})\mathbf{V} + \mathbf{I}^*\mathrm{diag}(\mathbf{L})\mathbf{I}\right)$$
$$= \Re\mathbf{I}^* P_\Gamma^t \mathbf{f} e^{2\pi\iota\alpha t} - \mathbf{V}^*\mathrm{diag}(\mathbf{G})\mathbf{V}.$$

The right hand side, which has the form of power in minus power out, corresponds perfectly with the right hand side of (21). The calculation shows that the dynamics of energy for the entire lattice can be understood by observing boundary phenomena only; this implies that, locally, in the interior of the lattice, energy is conserved.

We also compute the time evolution of the total charge of the discrete system (17):

$$\frac{\mathrm{d}}{\mathrm{d}t}\mathbf{1}^t\mathrm{diag}(\mathbf{C})\mathbf{V} = \mathbf{1}^t\mathfrak{B}\mathbf{I} - \mathbf{1}^t\mathrm{diag}(\mathbf{G})\mathbf{V}$$
$$= \sum_{j\in\Gamma} I_j - \sum_{k\in\mathfrak{G}} G_k V_k.$$

This has the form of current in minus current out, corresponding perfectly with the right hand side of (22).

IV. SEPARATION OF VARIABLES SOLUTION

In this section, we use separation of variables to develop the exact, steady-state solution of (1) for constant ϵ and μ. We begin by assuming harmonic time-dependence of the fields,

$$E(x, y, t) = \tilde{E}(x, y)e^{2\pi\iota\alpha t}, \quad \Lambda(x, y, t) = \tilde{\Lambda}(x, y)e^{2\pi\iota\alpha t},$$

in which case system (1) reduces to

$$(\nabla^2 + k^2)\tilde{E} = 0 \tag{23a}$$
$$\tilde{E}(0, y) = f(y) \tag{23b}$$
$$\frac{\partial\tilde{E}}{\partial n} + \iota k z\tilde{E} = 0 \qquad \text{on } \partial\Omega \setminus \overline{\Gamma}, \tag{23c}$$

where $k^2 = \mu\epsilon(2\pi\alpha)^2$ and $z = \sigma\sqrt{\mu/\epsilon}$. We now assume a solution of the form $\tilde{E}(x, y) = \rho(x)\psi(y)$. Inserting this into the Helmholtz equation (23a), we split the problem as follows:

$$\frac{\rho''(x)}{\rho(x)} + k^2 = -\frac{\psi''(y)}{\psi(y)} = \lambda. \tag{24}$$

This yields a non-selfadjoint problem for a complex eigenfunction $\psi(y)$ and a complex eigenvalue λ:

$$\psi''(y) = -\lambda\psi(y) \tag{25a}$$
$$\psi'(L) + \iota k z\psi(L) = 0 \tag{25b}$$
$$-\psi'(0) + \iota k z\psi(0) = 0 \tag{25c}$$

We say that $\phi(y)$ solves the adjoint problem if it satisfies:

$$\phi''(y) = -\lambda\phi(y) \tag{26a}$$
$$\phi'(L) - \iota k z\phi(L) = 0 \tag{26b}$$
$$-\phi'(0) - \iota k z\phi(0) = 0 \tag{26c}$$

We list without proof the properties of the eigenvalue problem that are most relevant to developing a separation of variables solution. For details, refer to [34], [35].

1) (25) is not a Sturm-Liouville problem because the boundary conditions are not self-adjoint.
2) If the eigenpair (λ_1, ψ) solves (25), the eigenpair (λ_2, ϕ) solves (26), and $\lambda_1 \neq \overline{\lambda_2}$, then ψ and ϕ are orthogonal with respect to the L^2 inner product:

$$\langle \psi, \phi \rangle := \int_0^L \psi(y)\overline{\phi(y)}\, dy = 0.$$

3) If the eigenpair (λ, ψ) solves (25), then the eigenpair $(\overline{\lambda}, \overline{\psi})$ solves (26). In this case, $\langle \psi, \overline{\psi} \rangle \neq 0$.
4) The eigenvalues are discrete, simple, and live in the first quadrant of $\mathbb{C}$.
5) The set $\{\psi_n\}_{n=1}^{\infty}$ is a complete basis of $L^2([0, L])$.
6) As $n \uparrow \infty$, the eigenfunctions ψ_n are increasingly oscillatory and alternatingly even and odd about $y = L/2$.

Note that

$$\psi_n(y) = e^{\imath\sqrt{\lambda_n}y} + \frac{\sqrt{\lambda_n} - kz}{\sqrt{\lambda_n} + kz}e^{-\imath\sqrt{\lambda_n}y} \qquad (27)$$

is an eigenfunction of (25) as long as λ_n solves the transcendental equation

$$e^{2\imath\sqrt{\lambda}L} = \left(\frac{\sqrt{\lambda} - kz}{\sqrt{\lambda} + kz}\right)^2. \qquad (28)$$

Using this and the above properties, we can derive the solution of (23). We expand the left-hand side boundary condition via

$$f(y) = \sum_{n=1}^{\infty} c_n \psi_n(y).$$

Taking inner products, we find

$$c_m = \frac{\langle f, \phi_m \rangle}{\langle \psi_m, \phi_m \rangle}.$$

We return to (24) and see that $\rho(x)$ must satisfy

$$\rho_n''(x) = (\lambda_n - k^2)\rho_n(x) \qquad (29a)$$
$$\rho_n(0) = 1 \qquad (29b)$$
$$\rho_n'(M) + \imath kz\rho_n(M) = 0 \qquad (29c)$$

The solution of (29) is

$$\rho_n(x) = \frac{q}{q+1}e^{\sqrt{\lambda_n - k^2}x} + \frac{1}{q+1}e^{-\sqrt{\lambda_n - k^2}x},$$

where

$$q = \frac{\sqrt{\lambda_n - k^2} - \imath kz}{\sqrt{\lambda_n - k^2} + \imath kz}e^{-2\sqrt{\lambda_n - k^2}M}.$$

The solution of (23) is then

$$\tilde{E}(x, y) = \sum_{n=1}^{\infty} c_n \rho_n(x)\psi_n(y). \qquad (30)$$

A. Solving (28) for the eigenvalues

Let $\sqrt{\lambda} = a + \imath b$. Taking the square root of both sides of (28) and then splitting the resulting equation into its real and imaginary parts leads us to the fixed point iteration scheme

$$\begin{pmatrix} a_{j+1} \\ b_{j+1} \end{pmatrix} = F_n \begin{pmatrix} a_j \\ b_j \end{pmatrix},$$

where

$$F_n \begin{pmatrix} a \\ b \end{pmatrix} = \begin{pmatrix} \dfrac{n\pi}{L} + \dfrac{1}{L}\tan^{-1}\dfrac{2bkz}{a^2 + b^2 - k^2z^2} \\ -\dfrac{1}{2L}\log\dfrac{(a^2 + b^2 - k^2z^2)^2 + (2bkz)^2}{((a + kz)^2 + b^2)^2} \end{pmatrix}.$$

Let D be the disc $\{w \in \mathbb{C} \mid |w - (kz)^2| < 2kz/L\}$. If the eigenvalue λ_n satisfies $\lambda_n \notin D$, it can be shown using the contraction mapping principle that F_n has a unique fixed point (a, b) where $aL/\pi \in (n - 1/2, n + 1/2)$. In practice, we find that this means that applying F_n for $1 \leq n \leq N$, one obtains all eigenvalues with real parts in the interval $(0, ((N + 1/2)\pi/L)^2)$ except possibly for one eigenvalue that can be found by applying Newton's method in the disc D.

The eigenvalues found in this way constitute the full spectrum of (25). Note that as $n \uparrow \infty$, the eigenvalues have the asymptotic form

$$\sqrt{\lambda_n} \sim \frac{n\pi}{L} + \imath\frac{2kz}{n\pi}. \qquad (31)$$

B. The transfer function on the rectangle

We define the transfer function $T(f)$ to be the mapping from the left boundary condition $f(y)$ to the solution $\tilde{E}(M, y)$ on the right boundary, i.e.,

$$T(f) = \sum_{n=1}^{\infty} \frac{\langle \overline{\psi}_n, f \rangle}{\langle \overline{\psi}_n, \psi_n \rangle}\rho_n(x = M)\psi_n(y). \qquad (32)$$

Let $\mu_n = \sqrt{\lambda_n - k^2}$. Using (30), we derive

$$\rho_n(M) = \frac{2\mu_n e^{-\mu_n M}}{(\mu_n + \imath kz) + (\mu_n - \imath kz)e^{-2\mu_n M}}. \qquad (33)$$

Combining this with (31), we see that for large n,

$$|\rho_n(M)| \sim e^{-n\pi M/L}. \qquad (34)$$

Since $\langle \overline{\psi}_m, T(f) \rangle = \langle \overline{\psi}_m, f \rangle \rho_n(M)$, the upshot of (34) is that the transfer function (32) does not conserve energy, since the large n modes of $f(y)$ are severely damped. Also, the solution on the right boundary will be much smoother than $f(y)$.

V. NUMERICAL IMPLEMENTATION AND CONVERGENCE

In this section, we discuss the application of the finite volume method to two test problems. Throughout the finite volume solution, we set $\eta = 1$. We use V to denote the components of the finite volume solution u that represent voltages at lattice nodes.
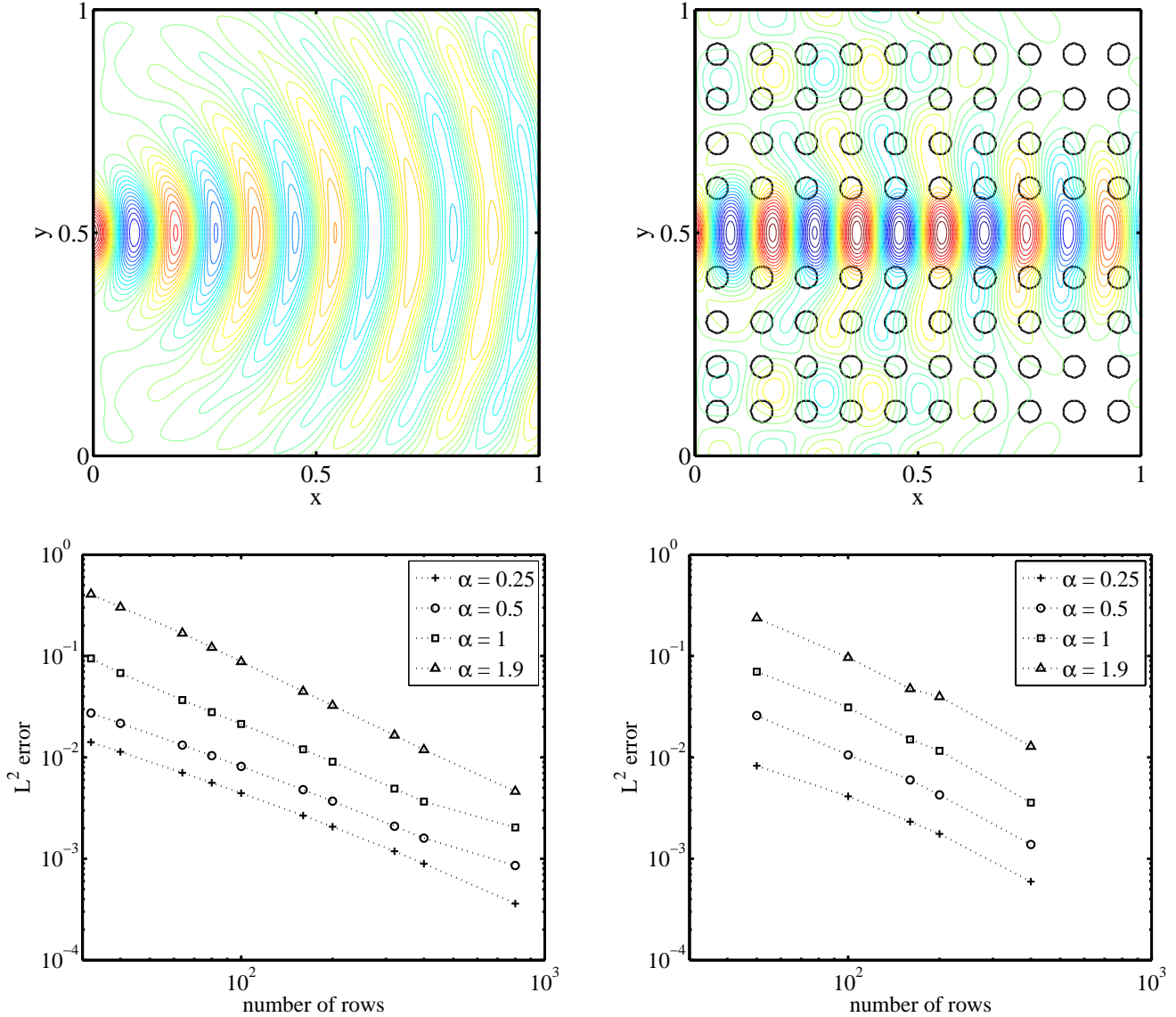
Fig. 2. The left panels show results from simulations of a homogeneous medium with $\epsilon = 9$ and $\mu = 1$ as in Sec. V-A. The right panels show results from simulations of an inhomogeneous medium as in Sec. V-B. The black circles in the upper-right panel mark the parts of the medium within which $\epsilon = 1$; otherwise, $\epsilon = 9$. Again, $\mu = 1$ everywhere. The same Gaussian boundary forcing at angular frequency $\alpha = 1.9$ is applied in both problems. The numerically computed real part of the electric field is indicated by the color contour plots. Note that the effect of the periodic array with linear defect is to confine the electromagnetic field and not allow it to diffract into the rest of the domain as in the homogeneous medium. The lower panels show the results of a convergence study in the form of log-log plots of the L^2 error between numerically computed solutions and a reference solution, as a function of the number of lattice rows. In the lower-left panel, the reference solution is a 50-mode truncation of the exact solution, while in the lower-right panel, the reference solution is the finite volume solution on an 800×800 lattice. The lower panels both show four curves, one for each indicated value of the angular frequency α. All eight curves have best-fit slope less than -1, indicating first-order convergence.

A. Homogeneous medium

For the separation of variables solution, we use (30), truncated at $n = 50$ modes, to produce a function $\tilde{E}(x, y)$. When we compare $\tilde{E}(x, y)$ against V_k, we average $\tilde{E}(x, y)$ over the cell Ω_k, following (11)—we denote the the averaged separation of variables solution by $\overline{E}$.

We focus on Gaussian boundary data $f(y) = e^{-a(y-1/2)^2}$ with $a = 150$ on the square domain with $M = L = 1$. We set $\epsilon = 9$ and $\mu = 1$. The finite volume solution of this problem at $\alpha = 1.9$ on a 400×400 lattice is given in the upper-left panel of Fig. 2.

For four different values of α, we compare the separation of variables solution to the finite volume solution V_m on an $m \times m$ lattice where $m = 20, 32, 40, 64, 80, 100, 160, 200, 320, 400,$ and 800. The lower-left panel of Fig. 2 shows a log-log plot of the L^2 error $\|V_m - \overline{E}\|_2$ versus m. When α equals 0.25, 0.5, 1.0, and 1.9, the least squares fit to the data gives slopes of, respectively, -1.10, -1.09, -1.27, and -1.36, indicating first-order convergence.

B. Periodic medium with a linear defect

We now consider a medium, modeled after a photonic crystal device [36], that consists of a periodic array of low index circular inclusions with a linear defect. The permittivity outside the inclusions is $\epsilon = 9$ and inside, $\epsilon = 1$. The domain is the square with $M = L = 1$. The distance between the centers of the circles is $1/10$ and each circle has radius $1/40$. The linear defect is created by simply removing a row of inclusions. The finite volume solution of this problem at $\alpha = 1.9$ on a 400×400 lattice is given in the upper-right panel of Fig. 2. As expected, the mode is confined to the defect, rather than diffracting as in the homogeneous medium.

We study the convergence of the finite volume method for this inhomogeneous medium by first obtaining a fine-scale finite volume solution V_{fine} on an 800×800 lattice. For the four values of α mentioned above, we compare this solution to the finite volume solution V_m on an $m \times m$ lattice for $m = 50$, 100, 200, 400. A log-log plot of $\|V_m - V_{\text{fine}}\|_2$ versus m is given in the lower-right panel of Fig. 2. A least squares fit of the error gives slopes of, respectively, -1.25, -1.39, -1.42, and -1.39, indicating first-order convergence.

VI. Conclusion

We have derived a physically motivated finite volume method for a planar Maxwell system. The method is easy to implement. Here we have done so to obtain the frequency domain solution of two problems with harmonic time-dependence. However, the system (17) obtained after spatial discretization could be used with a time-stepping scheme to solve an initial value problem in the time domain. Note that to find a steady-state solution through time stepping that is as accurate as the solutions we obtained, one would require a temporal discretization with first-order global error. This typically means that the time-stepping scheme must be at least second-order accurate.

To demonstrate convergence, we compared numerical solutions with a separation of variables solution for constant ϵ and μ. Note that it is possible to generalize the separation of variables solution in Sec. IV to handle separable ϵ and μ.

The choice of discretization in Sec. II does not require smoothness of ϵ and μ. In other words, an advantage of the first-order method proposed here is that discontinuous material parameters can be handled readily. A goal for future work is to extensively test how roughness and/or short-wavelength oscillations in the coefficients ϵ and μ affect the performance of the finite volume method, and to compare the finite volume method to other frequency-domain methods for such problems.

Appendix A
An idealized physical configuration

In this section, we describe an idealized physical configuration in which the (H_1, H_2, E) polarized mode is an exact solution of Maxwell's equations and interpret the finite volume method derived in Sec. II in this context. The idea of formulating more systematic relationships between circuit- and field-theoretic concepts stems from [37].

We consider two perfectly conducting plates that are infinite in extent in the $\hat{x}$ and $\hat{y}$ directions and separated by a distance $\eta > 0$ in the $\hat{z}$ direction. Between the plates is a medium with parameters ϵ and μ that may vary in the $\hat{x}$ and $\hat{y}$ directions, but are constant in the $\hat{z}$ direction. Between the plates, the electric and magnetic fields satisfy Maxwell's equations with no free charge or currents. The boundary conditions on the plates are:

$$\hat{n} \times \vec{E} = 0, \qquad \hat{n} \cdot \vec{B} = 0 \tag{35a}$$

$$\hat{n} \cdot \vec{D} = \rho_s, \qquad \hat{n} \times \vec{H} = \vec{j}_s. \tag{35b}$$

where ρ_s and $\vec{j}_s$ are the surface charge and surface current. Here, $\hat{n} = \hat{z}$ for the upper surface and $\hat{n} = -\hat{z}$ for the lower surface. The $\big(H_1(x, y, t), H_2(x, y, t), E(x, y, t)\big)$ polarized mode automatically satisfies (35a). The last two boundary conditions reduce to

$$\epsilon E = \rho_s, \qquad \Lambda = (j_s^1, j_s^2),$$

where, as before, $\Lambda = (-H_2, H_1)$. Evaluating the line integral of $\nabla \cdot (\epsilon E)$ connecting $(x, y, 0)$ and (x, y, η), we find that the charge density on the two plates at fixed (x, y) are equal in magnitude but have opposite signs. We now identify the charge $Q_k(t)$, defined by (2), with the area integral over Ω_k of the surface charge on the top plate. For constant ϵ, (3) agrees with the capacitance between two parallel plates of area $|\Omega_k|$ separated by a distance η: $\epsilon |\Omega_k| / \eta$. The electrostatic potential difference between the two plates at position (x, y) can be defined by

$$V(x, y, t) = \int_0^\eta E(x, y, t) \, \mathrm{d}z = \eta E(x, y, t).$$

The approximation of the quantity $V_k \equiv Q_k / C_k$ in (11) is precisely the average value $V(x, y, t)$ on Ω_k. Thus the approximation made in (11) can be interpreted as an electrostatic approximation.

Continuity of charge requires that for any rectangular region Ω_k on the top conducting plate, we must have

$$\frac{\mathrm{d}}{\mathrm{d}t} \int_{\Omega_k} \rho_s(x, y) \, \mathrm{d}\vec{x} = -\oint_{\partial \Omega_k} j_s \, \mathrm{d}\ell = -\oint_{\partial \Omega_k} \Lambda \, \mathrm{d}\ell.$$

Thus the line integral of the surface current over one segment of $\partial \Omega_k$ is equivalent to the current defined by (7), and the continuity equation is equivalent to Kirchhoff's law (8).

Suppose there is a surface current between two cells in the $\hat{x}$ direction. This induces a magnetic field in the $\hat{y}$ direction just below the top plate. If the current increases (resp. decreases), then the field will also increase (resp. decrease). By Faraday's law of induction, this increasing (resp. decreasing) field will induce an electromotive force in the $\hat{x}$ direction (resp. $-\hat{x}$ direction) proportional to μ. This is Kirchhoff's law (12).

REFERENCES

[1] J. R. Whinnery and S. Ramo, "A new approach to the solution of high-frequency field problems," *Proc. I. R. E.*, vol. 32, pp. 284–288, 1944.

[2] G. Kron, "Equivalent circuit of the field equations of Maxwell—I," *Proc. I. R. E.*, vol. 32, no. 5, pp. 289–299, 1944.

[3] J. R. Whinnery, C. Concordia, W. Ridgway, and G. Kron, "Network analyzer studies of electromagnetic cavity resonators," *Proc. I. R. E.*, vol. 32, pp. 360–367, 1944.

[4] L. Brillouin, *Wave Propagation in Periodic Structures. Electric Filters and Crystal Lattices*, ser. International Series in Pure and Applied Physics. New York, NY: McGraw-Hill, 1946.

[5] C. Christopoulos, *The Transmission-Line Modeling Method (TLM)*. Piscataway, NJ: IEEE Press, 1995.

[6] W. K. Gwarek, "Analysis of an arbitrarily-shaped planar circuit a time-domain approach," *IEEE Trans. Microw. Theory Tech.*, vol. 33, pp. 1067–1072, 1985.

[7] K. Guillouard, M. F. Wong, V. F. Hanna, and J. Citerne, "A new global time-domain electromagnetic simulator of microwave circuits including lumped elements based on finite-element method," *IEEE Trans. Microw. Theory Tech.*, vol. 47, pp. 2045–2049, 1999.

[8] L. B. Felsen, M. Mongiardo, and P. Russer, *Electromagnetic Field Computation by Network Methods*. New York, NY: Springer-Verlag, 2008.

[9] W. J. R. Hoefer, "The Transmission-Line Matrix method—theory and applications," *IEEE Trans. Microw. Theory Tech.*, vol. 33, pp. 882–893, 1985.

[10] C. Christopoulos, *The Transmission-Line Modeling (TLM) Method in Electromagnetics*. San Rafael, CA: Morgan & Claypool, 2006.

[11] Y. Ko, N. Yoshida, and I. Fukai, "Three-dimensional analysis of a cylindrical waveguide converter for circular polarization by the spatial network method," *IEEE Trans. Microw. Theory Tech.*, vol. 38, pp. 912–918, 1990.

[12] H. Satoh, N. Yoshida, S. Kitayama, and S. Konaka, "Analysis of 2-D frequency converter utilizing compound nonlinear photonic-crystal structure by condensed node spatial network method," *IEEE Trans. Microw. Theory Tech.*, vol. 54, pp. 210–215, 2006.

[13] N. K. Madsen and R. W. Ziolkowski, "Numerical solution of Maxwell's equations in the time domain using irregular nonorthogonal grids," *Wave Motion*, vol. 10, no. 6, pp. 583–596, 1988.

[14] V. Shankar, W. F. Hall, and A. H. Mohammadian, "A time-domain differential solver for electromagnetic scattering problems," *Proc. IEEE*, vol. 77, no. 5, pp. 709–721, 1989.

[15] N. K. Madsen and R. W. Ziolkowski, "A three-dimensional modified finite volume technique for Maxwell's equations," *Electromagnetics*, vol. 10, no. 1, pp. 147–161, 1990.

[16] V. Shankar, A. H. Mohammadian, and W. F. Hall, "A time-domain, finite-volume treatment for the Maxwell equations," *Electromagnetics*, vol. 10, no. 1–2, pp. 127–145, 1990.

[17] I. E. Lager, E. Tonti, A. T. de Hoop, G. Mur, and M. Marrone, "Finite formulation and domain-integrated field relations in electromagnetics—a synthesis," *IEEE Trans. Magn.*, vol. 39, pp. 1199–1202, 2003.

[18] C. Fumeaux, D. Baumann, and R. Vahldieck, "Advanced FVTD simulation of dielectric resonator antennas and feed structures," *ACES Journal*, vol. 19, pp. 155–164, 2004.

[19] D. Baumann, M. Gimersky, C. Fumeaux, and R. Vahldieck, "Accuracy considerations of the FVTD method for radiating structures," in *European Microwave Conference, 2005*, vol. 2, 2005.

[20] K. Krohne, D. Baumann, C. Fumeaux, E.-P. Li, and R. Vahldieck, "Frequency-domain finite-volume simulations," in *European Microwave Conference, 2007*, 2007, pp. 158–161.

[21] E. T. Chung, Q. Du, and J. Zou, "Convergence analysis of a finite volume method for Maxwell's equations in nonhomogeneous media," *SIAM J. Numer. Anal.*, vol. 41, no. 1, pp. 37–63, 2003.

[22] E. T. Chung and B. Engquist, "Convergence analysis of fully discrete finite volume methods for Maxwell's equations in nonhomogeneous media," *SIAM J. Numer. Anal.*, vol. 43, no. 1, pp. 303–317, 2005.

[23] F. Hermeline, "A finite volume method for solving Maxwell equations in inhomogeneous media on arbitrary meshes," *C. R. Acad. Sci. Paris Sr. I Math.*, vol. 339, no. 12, pp. 893–898, 2004.

[24] F. Hermeline, S. Layouni, and P. Omnes, "A finite volume method for the approximation of Maxwell's equations in two space dimensions on arbitrary meshes," *J. Comput. Phys.*, vol. 227, no. 22, pp. 9365–9388, 2008.

[25] F. Edelvik, "Analysis of a finite volume solver for Maxwell's equations," in *Finite volumes for complex applications II*. Hermes Sci. Publ., Paris, 1999, pp. 141–148.

[26] S. D. Gedney, J. A. Roden, N. K. Madsen, A. H. Mohammadian, W. F. Hall, V. Shankar, and C. Rowell, "Explicit time-domain solutions of Maxwell's equations via generalized grids," in *Advances in Computational Electrodynamics*, ser. Artech House Antenna Lib. Boston, MA: Artech House, 1998, pp. 163–262.

[27] Z. J. Wang, A. J. Przekwas, and Y. Liu, "A FV-TD electromagnetic solver using adaptive Cartesian grids," *Comput. Phys. Comm.*, vol. 148, no. 1, pp. 17–29, 2002.

[28] E. Abenius, U. Andersson, F. Edelvik, L. Eriksson, and G. Ledfelt, "Hybrid time domain solvers for the Maxwell equations in 2D," *Internat. J. Numer. Methods Engrg.*, vol. 53, no. 9, pp. 2185–2199, 2002.

[29] R. J. LeVeque, *Finite Volume Methods for Hyperbolic Problems*, ser. Cambridge Texts in Applied Mathematics. Cambridge: Cambridge University Press, 2002.

[30] H. S. Bhat and B. Osting, "Diffraction on the two-dimensional square lattice," *SIAM J. Appl. Math.*, vol. 70, no. 5, pp. 1389–1406, 2009.

[31] ——, "Discrete diffraction in two-dimensional transmission line meta-materials," *Microw. Opt. Tech. Lett.*, vol. 52, no. 3, pp. 721–725, 2010.

[32] B. Engquist and A. Majda, "Absorbing boundary conditions for numerical simulation of waves," *Proc. Nat. Acad. Sci. U.S.A.*, vol. 74, no. 5, pp. 1765–1766, 1977.

[33] L. R. Foulds, *Graph Theory Applications*, ser. Universitext. New York: Springer-Verlag, 1992.

[34] E. A. Coddington and N. Levinson, *Theory of Ordinary Differential Equations*. New York: McGraw-Hill, 1955.

[35] D. S. Cohen, "Separation of variables and alternative representations for non-selfadjoint boundary value problems," *Comm. Pure Appl. Math.*, vol. 17, pp. 1–22, 1964.

[36] J. D. Joannopoulos, S. G. Johnson, J. N. Winn, and R. D. Meade, *Photonic Crystals: Molding the Flow of Light*, 2nd ed. Princeton, NJ: Princeton University Press, 2008.

[37] R. B. Adler, L. J. Chu, and R. M. Fano, *Electromagnetic Energy Transmission*. John Wiley & Sons, 1960.

Harish S. Bhat received the A.B. degree in Mathematics from Harvard University (Cambridge, MA) in 2000, and the Ph.D. degree in Control and Dynamical Systems from the California Institute of Technology (Pasadena, CA) in 2005. From 2005 to 2007, he held a postdoctoral position as the Chu Assistant Professor in the Department of Applied Physics and Applied Mathematics at Columbia University (New York, NY). From 2007 to 2008, he was on the faculty in the Department of Mathematics at Claremont McKenna College (Claremont, CA). He joined the School of Natural Sciences at the University of California, Merced (Merced, CA) as an Assistant Professor in July, 2008. His research interests include developing perturbative and numerical methods to understand linear and nonlinear wave propagation in a variety of media, e.g., networks of electrical oscillators. He is also interested in applying optimization methods to synthesize networks with prescribed properties.

Braxton Osting received B.S. degrees in Mathematics, Physics, and Applied Mathematics from the University of Washington (Seattle, WA) in 2005 and the Ph.D. degree in Applied Mathematics from Columbia University (New York, NY) in 2011. His research interests include analytical and computational methods to study mathematical models of wave phenomena in media where inhomogeneity, nonlinearity, dispersion, or geometry affect propagation. He is particularly interested in the strategy of using such a model together with an efficient optimization method to design the media to control some aspect of the wave propagation for novel applications.